Electric Power Systems Research 262 (2027) 113544



Contents lists available at ScienceDirect

Electric Power Systems Research

journal homepage: www.elsevier.com/locate/epsr



Augmenting distance protection with a data-based approach to fault classification under uncertainty ⋆

Sarah Anhaus *, Arlind Damjani, Willem Leterme

IAEW of RWTH Aachen University, Aachen, Germany

ARTICLE INFO

Keywords:
Distance protection
Fault classification
Machine learning
Random forest

ABSTRACT

The increasing use of grid-connected converters challenges the dependability and security of distance protection. Unlike synchronous machines, converters provide limited and control-dependent fault currents distorting apparent impedance trajectories. In combination with low short-circuit strength and varying pre-fault operating states, this increases the risk of misoperation of conventional distance relays, particularly near the Zone 1 boundary. This work applies Random Forest classification to the IEEE 14-bus system under varying system and operating conditions. The classifier reaches 93.6% accuracy for 3ph-gnd faults and reveals systematic misclassifications. SHAP analysis identifies apparent impedance, pre-fault power flow and system strength as dominant drivers, linking data-driven results to classical protection concepts. Threshold and receiver–operating–characteristic analyses show that optimal operating points deviate from fixed reach settings and shift the balance between dependability and security. A 90.08% reach performs best for 3ph-gnd faults, while 77.58% improves 1ph-gnd performance, indicating that static geometric zones cannot ensure balanced protection performance.

1. Introduction

The energy transition is driving the integration of converter-based renewable generation into transmission networks [1]. As the share of synchronous machines declines and grid-connected converters (GCCs) become more prevalent, the system's dynamic behaviour, particularly under fault conditions, changes fundamentally [2]. GCCs exhibit current-limited fault responses, lack inertia and voltage stiffness and rely on fast control dynamics. As a result, their fault behaviour is nonlinear and highly variable [3]. Instead of large and predictable short-circuit currents, converters inject smaller and control-dependent fault currents whose characteristics depend on pre-fault load flow, converter control strategy and grid strength. These dependencies not only affect fault current magnitudes but also alter the voltage-current relationship seen by a relay. Consequently, the apparent impedance trajectories in the R–X plane become distorted and operating-point dependent. Traditional distance relays, designed under strong-grid assumptions, therefore often struggle to ensure both security and dependability in converter-dominated environments [4], as fault classification based on fixed impedance thresholds becomes increasingly unreliable. Experimental and simulation studies empirically confirm such deviations of impedance trajectories from their expected characteristics and document the associated increase in misoperations [1,2,4]. These deviations become particularly pronounced in grids with low short-circuit capacity and in converter-interfaced renewable plants [5]. Although adaptive fault-classification strategies have been proposed to mitigate these risks [6], broader analyses indicate that converter-induced variability reveals structural limitations of conventional protection schemes [7]. Key challenges include:

- **Impedance distortion:** Converter fault infeed reshapes the apparent impedance trajectory in the R–X plane, reducing the reliability of fixed zone boundaries [6,8].
- **Reduced fault discrimination in weak grids:** Low short-circuit strength decreases fault current levels and impairs the separation of in-zone and out-of-zone faults, particularly near zone limits [9].
- **Sensitivity to operating conditions:** Variations in system and control parameters shift the impedance locus, leading to inconsistent classification of identical fault locations and weakening static zone robustness [5].

To address these challenges, modern protection schemes should incorporate the following requirements:

1) **Context awareness:** Protection logic should include indicators such as short-circuit power (SCP) or short-circuit ratio (SCR) to explicitly reflect system strength and converter influence.

⋆ Submitted to the 24th Power Systems Computation Conference (PSCC 2026).

* Corresponding author.
E-mail address: s.anhaus@iaew.rwth-aachen.de (S. Anhaus).

https://doi.org/10.1016/j.epsr.2026.113544
Received 10 October 2025; Received in revised form 28 February 2026; Accepted 20 June 2026
Available online 27 June 2026
0378-7796/© 2026 The Authors. Published by Elsevier B.V. This is an open access article under the CC BY license (http://creativecommons.org/licenses/by/4.0/).

2) **Adaptive classification with boundary robustness:** Impedance zones should adapt to changing fault and grid conditions rather than relying solely on fixed thresholds, thereby maintaining both security and dependability. This includes reliable handling of faults near zone limits, for example through delayed tripping.

Artificial intelligence (AI) and machine learning (ML) have been increasingly investigated for power system protection. Early neural network-based relay concepts date back to the 1990s [10,11] and were later summarized for transmission fault detection and classification [12]. With the transition toward grids with high converter shares, ML and deep learning approaches have gained renewed attention, as highlighted in recent surveys [13–15]. These works emphasize the growing reliance on data-driven methods to cope with nonlinear system behaviour and reduced short-circuit strength. Correspondingly, protection schemes based on supervised learning have been proposed for microgrids, networks with high penetration of converter-interfaced distributed generation, series-compensated lines, and hybrid HVAC/HVDC systems [16–20]. While many of these approaches report high classification accuracy, they primarily emphasise predictive performance rather than protection-oriented evaluation. System strength, proximity to impedance boundaries and converter-induced uncertainty are often not analysed systematically, and consistency with classical protection criteria such as security and dependability is rarely assessed explicitly.

From a methodological perspective, various machine learning techniques can be applied, including Support Vector Machines, k-Nearest Neighbors and Deep Neural Networks (DNNs) [21]. Although deep learning models perform well in high-dimensional settings [14], often achieving high predictive accuracy, they typically require large datasets and extensive hyperparameter tuning. More critically, the limited interpretability of complex neural architectures conflicts with the transparency requirements of protection engineering. In safety-critical applications, decisions must be traceable and systematically validated against classical criteria such as security and dependability, making interpretability a prerequisite rather than an optional advantage. Against this background, Random Forests (RF), introduced by Breiman [22], offer a robust ensemble-based alternative. RF models are resistant to overfitting, operate reliably under noisy measurements and provide intrinsic feature importance measures [23]. This allows a quantitative analysis of how grid strength, loading conditions and impedance characteristics affect classification outcomes, in line with recent developments in explainable artificial intelligence for critical infrastructure systems [24,25].

Based on these considerations, this work proposes a supervised RF-based framework for distance protection under uncertain grid conditions. The approach integrates contextual indicators such as SCP to improve robustness near impedance zone boundaries. Protection performance is evaluated using confusion matrices and ROC analysis [21], enabling explicit assessment of security-dependability trade-offs. The main contributions of this work are:

- A protection-oriented uncertainty analysis quantifying how system strength and converter operating conditions affect apparent impedance behaviour.
- The development of operating-condition-aware decision regions moving beyond static geometric zone settings through supervised learning.
- A protection-focused evaluation framework explicitly incorporating dependability and security into classification and threshold selection.

Unlike purely accuracy-driven ML approaches, the proposed framework combines data-driven classification with classical protection principles to ensure engineering transparency and practical applicability in converter-dominated transmission grids. The paper is organised as follows: Chapter II analyses the behaviour of apparent impedance under varying system conditions. Chapter III describes the methodology. Chapter IV presents the case study and results, including interpretability analysis. Chapter V concludes with key findings and future work.

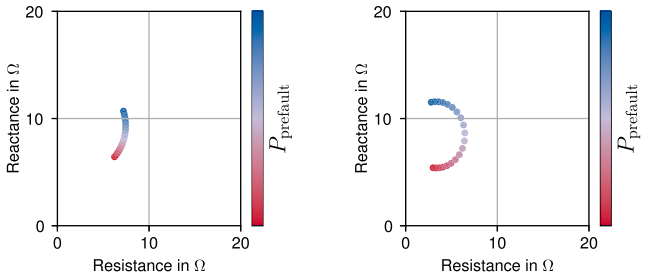


Fig. 1. Variation of P_{prefault} for different SCR levels (left: 5, right: 1). Color ranges from −2 GW (red) to +2 GW (blue). Fault location fixed at 80% of line length with $R_f = 3\ \Omega$.

2. Apparent impedance under system-dependent conditions

The apparent impedance is the central decision variable of distance protection and can be expressed under double-infeed conditions [26,27]

$$\underline{Z}_{\text{A}} = \left(\frac{x}{l}\right)\underline{Z}_{\text{L}} + R_{\text{F}} + \frac{\underline{I}_{\text{B}}}{\underline{I}_{\text{A}}} R_{\text{F}}, \tag{1}$$

where $\underline{Z}_{\text{L}}$ is the line impedance, R_{F} the fault resistance and $\underline{I}_{\text{A}}$, $\underline{I}_{\text{B}}$ the local and remote fault currents. The decisive influence lies in the last term of Eq. (1), which reflects the current contribution from the remote side. Using local Thevenin equivalents, the current ratio can be approximated [26]

$$\frac{\underline{I}_{\text{B}}}{\underline{I}_{\text{A}}} \approx \frac{\underline{E}_{\text{B}}}{\underline{E}_{\text{A}}} \frac{Z_{\text{th},A}}{Z_{\text{th},B}}, \tag{2}$$

so that its magnitude scales with the relative short-circuit powers and its angle follows the pre-fault voltage difference [27]. A reduction in system short-circuit power not only increases the sensitivity of the apparent impedance to remote infeed, but also decreases the robustness of the relay characteristic against operating-point variations [5]. Particularly in weak grids, even small fluctuations in the remote contribution can result in noticeable shifts of the apparent impedance, thereby reducing the dependability of Zone 1 operation [4]. Pre-fault conditions, such as load flow and bus voltage, further influence the voltage ratio $\frac{\underline{E}_{\text{B}}}{\underline{E}_{\text{A}}}$ and thereby shift the reference point of the impedance locus [26]. These dependencies imply that the apparent impedance is not solely a function of fault location, but also of the prevailing operating point, making protection reliability strongly scenario-dependent. The overall behaviour strongly depends on the generation mix, as the share between synchronous machines and converter-based resources determines both the amplitude and controllability of fault currents [1]. With increasing converter penetration, the variability of these contributions grows, producing a wide spread of possible impedance loci even for identical fault locations [3]. Converters reduce the effective short-circuit power and shape fault currents according to their control objectives [8].

Different control modes (e.g., current-priority or voltage-support) produce distinct fault injections that modify both the magnitude and phase of the remote-to-local current ratio [3]. As a result, the apparent impedance locus becomes controller-dependent and the safety margin to the Zone 1 boundary highly sensitive to both system conditions and converter control design, with direct implications for protection security and dependability.

2.1. Impedance sensitivity to operating conditions

To quantify the mechanisms described above, a minimal three-bus transmission system inspired by [26] is considered that captures the relevant interactions. Bus 1 is connected to Bus 2 via a 40 km protected

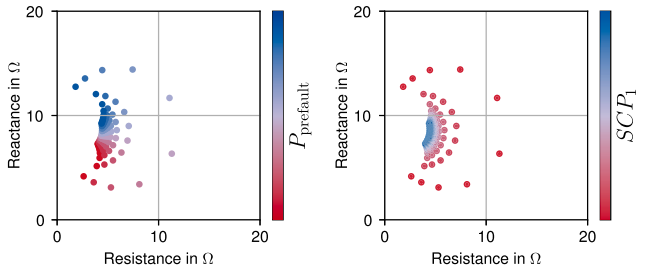


Fig. 2. Variation of P_{prefault} and SCP_1 for 3ph-gnd fault. Red indicates the minimum and blue the maximum of the respective parameter range.

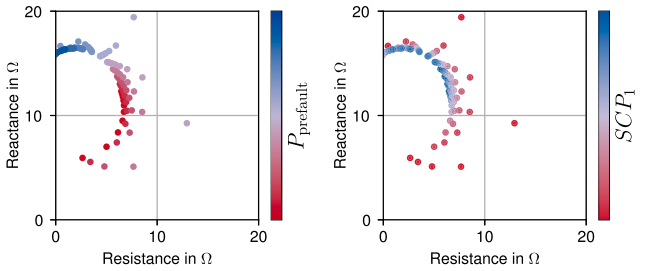


Fig. 3. Variation of P_{prefault} and SCP_1 for 1ph-gnd fault. Red indicates the minimum and blue the maximum of the respective parameter range.

line where faults are applied and hosts a GCC to explicitly examine its impact on fault behaviour. Pre-fault power flows are calculated with `pandapower` [28] and faults are introduced as lumped events by adapting the grid topology and adding a resistance. From simulated voltages and currents, the apparent impedance is obtained in the *R-X* plane for representative symmetric (three-phase-to-ground) and asymmetric (single-phase-to-ground) fault cases, hereafter denoted as 3ph-gnd and 1ph-gnd. Parameter variations cover P_{prefault} from −2 to +2 GW, short-circuit powers SCP_1 and SCP_2 from 1 to 10 GVA within the 380 kV grid and fault locations with x_f between [0, 100]% with fault resistances R_f in the range [0, 10] Ω. Unless stated otherwise, default values are $R_f = 3\,\Omega$, fault location at 80% of line length, $SCP = 3$ GVA and $P_{\text{prefault}} = 2$ GW. The apparent impedance depends on P_{prefault} under strong ($SCR = 5$) and weak ($SCR = 1$) conditions (see Fig. 1). The SCR level directly reflects the ratio of local to remote short-circuit power; for a reference injection of 2 GW this corresponds to $SCR = 1$. In strong grids, the impedance loci remain closely clustered around the line impedance and show only minor sensitivity to P_{prefault}.

By contrast, in weak grids the trajectories spread widely in the *R-X* plane. Their location depends strongly on the magnitude and sign of P_{prefault}: positive injections shift the locus to higher resistance, whereas low or negative injections lead to larger reactances. This confirms the analytical result in (1)-(2), where the local infeed term becomes dominant as the short-circuit strength decreases. Further, the two-factor-at-a-time (TAT) analysis in Figs. 2 and 3 extends this observation by combining variations of P_{prefault} and SCP_1 of Bus 1. Increasing SCP_1 systematically reduces the spread of the impedance, while variations of P_{prefault} shift the trajectories in both resistive and reactive directions. For 1ph-gnd faults, small or negative P_{prefault} values yield higher reactances and lower resistances, whereas in the 3ph-gnd case the effect is more pronounced along the resistive axis.

Overall, this pre-study confirms that the apparent impedance is not only determined by fault location and resistance, but is strongly shaped by the last term of the current ratio in (1). Higher infeed combined with low SCP_1 or faults located far from the relay, systematically displace the impedance locus. These findings, consistent with the analytical expressions in (1)-(2), underline that static zone settings cannot ensure robust operation in grids with higher shares of converters. The analysis is limited to a small set of parameter variations, yet already highlights the fundamental sensitivity of distance protection to operating-point conditions.

3. Methodology

The methodological framework investigates how distance protection decisions in Zone 1 are affected by varying system and operating conditions. A Random Forest classifier is applied as a binary decision model distinguishing whether a given fault lies inside or outside Zone 1. The model does not replace a protection function but quantifies how input parameters influence classification in protection-oriented terms. The tunable decision threshold refers to the classifier's posterior probability (not the relay reach setting) and can be adjusted to balance dependability and security. The feature vector is defined as

$$\mathbf{x} = \left[X_{\text{meas}}, R_{\text{meas}}, P_{\text{prefault}}, SCP_{\text{bus1}}, SCP_{\text{bus2}}, \phi_{\text{conv}}, k_{\text{conv}}\right]. \tag{3}$$

As defined in Eq. (3), it combines classical impedance quantities with selected contextual system indicators. Fault resistance R_f and fault location x_f are varied during data generation but are not included in the feature vector, as they are not directly observable by the relay and would introduce information leakage. The dataset comprises 10^5 simulated fault cases. Samples were randomly divided into 80% training and 20% test data using a fixed random seed to ensure reproducibility. Given the large dataset size and the moderate class balance (40% / 60%), no explicit class weighting or stratified split was applied. At this scale, statistical bias due to sampling is negligible, indicating no severe class imbalance. Preliminary experiments on smaller datasets ($\approx 10^3$ cases) were evaluated using 5-fold cross-validation to assess model stability under higher parameter variance and reduced sample size. For the final dataset, the variance induced by random sampling was considered negligible; therefore, a single hold-out split was deemed sufficient. Implementation details: Python 3.12.5, `pandapower` 3.0.0, `scikit-learn` 1.6.1, `shap` 0.48.0. The RF hyperparameters used throughout this study are summarized in Table 1.

Table 1
Random forest hyperparameters used for all experiments.

Hyperparameter	Value	Remark
$n_{\text{estimators}}$	100	Number of trees
criterion	gini	Split criterion based on Gini impurity
max_depth	10	Maximum tree depth
max_features	$\sqrt{d}$ ($d = 7$)	$\lfloor\sqrt{7}\rfloor = 2$ candidate features per split
min_samples_split	2	Minimum samples required to split an internal node
min_samples_leaf	1	Minimum samples required at a leaf node
bootstrap	True	Bootstrapped sampling for each tree
class_weight	None	No explicit class weighting applied
random_state	42	Fixed seed for reproducibility

3.1. Random forest application

RF is an ensemble learning method combining multiple decision trees trained on bootstrapped subsets of the data [22]. At each split, only a random subset of features is considered, reducing correlation between trees and improving generalisation performance [21,23]. Predictions are aggregated using majority voting. Owing to their robustness against noise, ability to handle nonlinear feature interactions, and resistance to overfitting, RFs are widely used for classification tasks [29]. Tree-based splits are invariant under monotonic feature transformations, so no feature scaling is required. In this study, the RF model was configured with $B = 100$ trees, a maximum depth of 10 and the Gini impurity criterion for split evaluation [22] (Table 1). Extensive hyperparameter optimisation was deliberately avoided, as the focus lies on interpretability and protection-oriented analysis rather than performance maximisation. Each tree T_b is trained on a bootstrapped dataset $D_b \subset D$. At each split, a

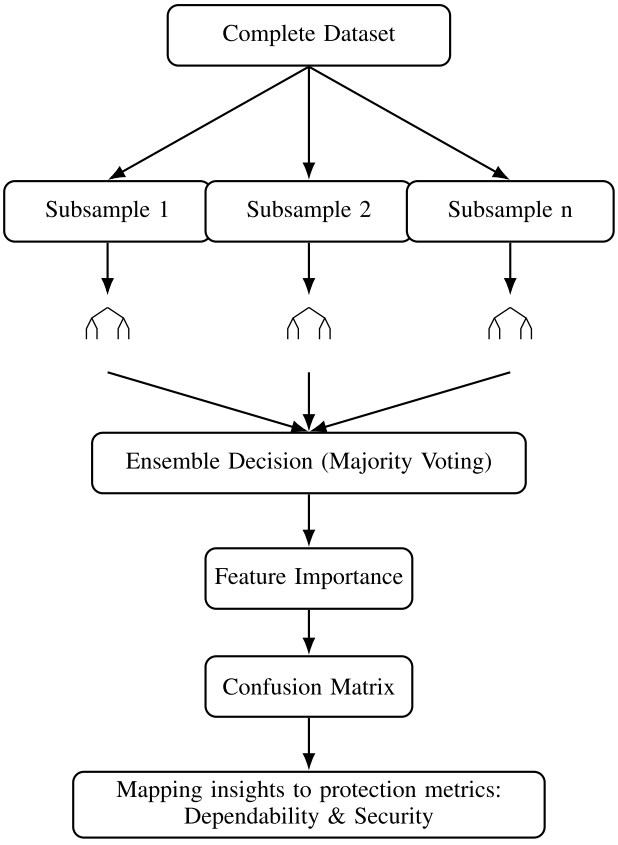


Fig. 4. Schematic workflow of the random forest framework for Zone 1 protection assessment.

random subset of features $\mathcal{F} \subset \mathcal{X}$ is evaluated. The ensemble prediction is defined as

$$\hat{y} = \text{mode}\{T_1(x), T_2(x), \ldots, T_B(x)\}, \tag{4}$$

where $T_b(x)$ denotes the predicted class of the bth tree. The overall workflow is illustrated in Fig. 4. The dataset is resampled via bootstrap aggregation, individual trees are trained independently, and their outputs are combined through majority voting. The resulting classification is subsequently analysed using feature importance measures and protection-oriented performance metrics.

3.2. Interpretation of RF classification outcomes

Beyond predictive performance, RF provides intrinsic feature importance measures based on impurity reduction across the ensemble. Features that consistently yield large reductions in Gini impurity are considered more influential in the decision process. To obtain sample-specific explanations, SHAP (SHapley Additive exPlanations) is employed [25,30]. Based on cooperative game theory, SHAP decomposes each prediction into additive feature contributions, ensuring that the total model output equals the sum of individual attributions [24]. This enables transparent tracing of how specific input parameters influence classification decisions. Beeswarm plots summarize SHAP values across samples, indicating both the relative importance of each feature and the direction of its impact. SHAP scatter plots further relate feature values to their SHAP contributions, revealing nonlinear dependencies and parameter interactions that increase misclassification risk [31]. These tools identify operating regions where classification uncertainty is elevated and where small parameter variations may significantly affect protection decisions.

3.3. Protection-oriented performance evaluation

To assess protection performance in Zone 1, misclassification must be distinguished from uncertainty. A misclassification occurs when an in-zone fault is predicted as outside, or vice versa, directly affecting protection reliability. Uncertainty is defined for cases where

$$0.1 < \hat{p}(\text{Zone1}|x) < 0.9,$$

as probabilities below 0.1 or above 0.9 indicate high-confidence predictions close to a definitive in-zone or out-of-zone decision. Values within this interval therefore represent operating conditions near the decision boundary. Classification outcomes are quantified using the confusion matrix, identifying true positives (TP), true negatives (TN), false positives (FP), and false negatives (FN) [21]. Dependability and security [26] are defined as

$$\text{Dependability} = \frac{\text{TP}}{\text{TP} + \text{FN}}, \tag{5}$$

$$\text{Security} = \frac{\text{TN}}{\text{TN} + \text{FP}}. \tag{6}$$

Receiver Operating Characteristic (ROC) analysis [32] evaluates classifier performance across probability thresholds by relating dependability (true positive rate) to $1 - \text{Security}$ (false positive rate). This enables systematic assessment of the security–dependability trade-off and supports threshold selection under varying operating conditions. From a methodological perspective, the RF framework offers a robust and interpretable modelling approach. However, the classification outcome inherently depends on the quality and representativeness of the underlying dataset. Practical applicability is primarily constrained by the availability and reliability of system variables in real-world protection environments.

4. Case study

The proposed methodology is evaluated on the IEEE 14-bus transmission system, which includes multiple generation sources, distinct load points and meshed interconnections. The line between Bus 1 and Bus 5 is selected as the protected element for Zone 1 evaluation.

4.1. Scenarios and simulation setup

For each fault type, 100,000 cases are simulated, yielding two datasets: one for 3ph-gnd and one for 1ph-gnd faults. Each dataset is evaluated separately to assess the influence of operating conditions on protection performance. In every case, the pre-fault operating point is computed, after which the fault is introduced as a lumped event by adapting the grid topology and adding a fault resistance. The resulting voltages and currents are used to calculate the apparent impedance in the R-X plane. These impedance quantities, together with contextual system indicators, form the classifier input. The IEEE 14-bus system consists of 14 buses and 20 transmission lines (Fig. 5). Bus 1 acts as the slack bus equipped with a grid-following GCC. Buses 2, 3, and 8 operate as generator buses with fixed injections, while Bus 6 hosts an additional GCC. The remaining buses (4–5 and 9–14) operate as PQ buses with active and reactive loads. Generator injections and load demands are varied within 150–300 MW and 30–80 Mvar. The short-circuit strength of the external networks in Buses 1 and 5 is systematically adjusted to analyse its impact on protection performance. Parameter ranges and default values are summarised in Table 2.

4.2. Random forest outcomes and feature interpretation

The Random Forest exhibits stable performance across different training splits, as indicated by the 5-fold cross-validation results (Table 4). The low standard deviations suggest consistent model behaviour and limited overfitting. On the independent test set, the classifier

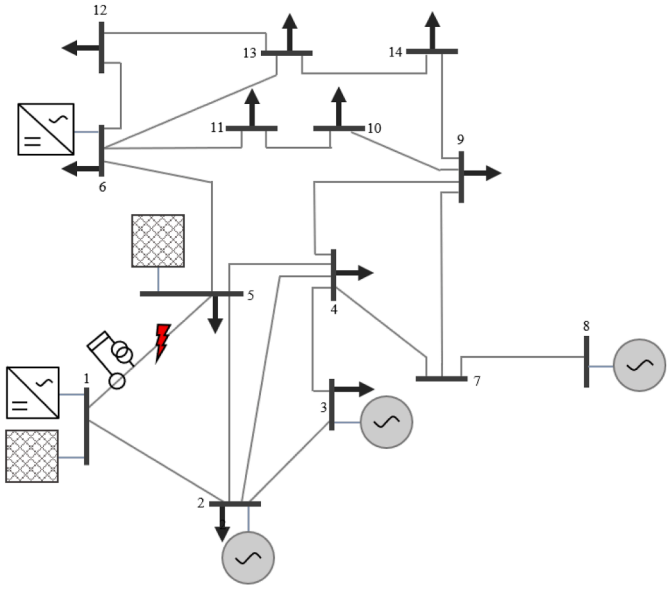


Fig. 5. IEEE 14-bus transmission system with fault location between Bus 1 and Bus 5.

Table 2
Parameter ranges and default values used for sensitivity analysis.

Category	Variable	Default	Range	Unit
Fault	x_F	50	[0, 100]	%
	R_F	5	[0, 10]	Ω
Line Impedance	R_L	0.0126	fixed	Ω/km
	X_L	0.2546	fixed	Ω/km
Grid	SCP_{bus1}	2	[1, 15]	GVA
	SCP_{bus5}	5	[1, 15]	GVA
	U_1	400	[360, 440]	kV
	U_2	400	[360, 440]	kV
Converter	P_{prefault}	0.2	[-2, 2]	GW
	ϕ_{conv}	$\pi/2$	$[0, \pi]$	rad
	k_{conv}	2	[1, 3]	–
Protection Zone	X_{bound}	$0.8X_L$	fixed	Ω
	R_{bound}	$0.8R_L + 7$	fixed	Ω

achieves an accuracy of 0.93 for 3ph-gnd faults and 0.89 for 1ph-gnd faults at a fixed decision threshold of 80% of line length (Table 3).

Table 3 summarises the detailed classification outcomes. For 3ph-gnd faults, the RF achieves 35,373 true positives, 4334 false negatives, 2277 false positives, and 58,018 true negatives. For 1ph-gnd faults, the classifier yields 30,496 true positives, 9211 false negatives, 1748 false positives, and 58,547 true negatives. Although the overall accuracies indicate strong classification performance, protection assessment requires analysing the distribution of residual errors. False negatives (missed in-zone faults) directly affect dependability, whereas false positives influence security. The confusion matrix therefore provides a protection-oriented evaluation beyond global accuracy. Feature importance rankings reveal the dominant role of X_{meas}, followed by R_{meas}, P_{prefault} and SCP_{bus1}, with slightly different weightings between 3ph-gnd and 1ph-gnd cases.

Fig. 6 illustrates a representative four-level decision tree extracted from the trained Random Forest for the 3ph-gnd dataset. The tree depth is limited to preserve interpretability while retaining the dominant split structure observed across the ensemble. The primary split on X_{meas} confirms its geometric importance for Zone 1 classification. Subsequent splits on R_{meas} and P_{prefault} demonstrate how apparent impedance quantities and converter operating conditions jointly influence the final decision. Although an individual tree does not reach the predictive performance of the full ensemble, it provides transparent insight into the hierarchical decision logic learned by the model. To further interpret the classification behaviour, SHAP values were computed. The beeswarm plots in Figs. 7 and 10 illustrate the distribution of feature contributions across all simulated fault cases. For 3ph-gnd faults, X_{meas} (0.42–0.54) exhibits the largest contribution, reflecting its fundamental geometric role in defining the decision boundary. R_{meas} (≈0.15), P_{prefault} (0.25–0.35), and SCP_{bus1} (≈0.07) follow with smaller but systematic contributions.

Table 3
Classifier performance and feature importance.

Outcome	3ph-gnd	1ph-gnd
Accuracy	0.93	0.89
Dependability	0.891	0.768
Security	0.962	0.971
TP	35,373	30,496
FN	4334	9211
FP	2277	1748
TN	58,018	58,547
Top Features	X_{meas} (0.585) R_{meas} (0.189) P_{prefault} (0.169) SCP_{bus1} (0.054)	X_{meas} (0.459) R_{meas} (0.235) P_{prefault} (0.228) SCP_{bus1} (0.076)

Table 4
5-fold stratified cross-validation results on the training set (mean ± std).

Metric	3ph-gnd	1ph-gnd
Accuracy	0.9329 ± 0.0023	0.8856 ± 0.0051
F1-score	0.9133 ± 0.0030	0.8417 ± 0.0073
Balanced Accuracy	0.9253 ± 0.0024	0.8650 ± 0.0056
ROC-AUC	0.9877 ± 0.0006	0.9704 ± 0.0017

This indicates that the apparent impedance components primarily determine the instantaneous classification boundary. However, P_{prefault} and SCP_{bus1} act as contextual parameters that systematically shift this boundary under varying operating conditions. High positive converter injections consistently displace cases toward the out-of-zone region, whereas increased short-circuit strength mitigates this displacement. A comparable pattern is observed for 1ph-gnd faults. X_{meas} and R_{meas} dominate the geometric classification, while P_{prefault} and SCP_{bus1} introduce systematic operating-point-dependent shifts. Weak-grid conditions amplify the influence of converter infeed, whereas stronger short-circuit support reduces the operating-point sensitivity of the classification outcome.

4.3. Misclassification analysis and critical parameter regions

The confusion matrix results show that misclassifications account for 11% of 3ph-gnd and 18% of 1ph-gnd cases. Since both fault types exhibit similar trends, the following discussion focuses on the 3ph-gnd case. Figs. 8 and 11 illustrate the distribution of misclassified samples. Each point corresponds to one fault case. The horizontal axis shows the varied parameter (P_{prefault} or SCP_{bus1}), while the color scale encodes X_{meas}. Two dominant clusters emerge. First, high positive P_{prefault} injections shift the apparent impedance toward higher resistance values, resulting in false negatives for in-zone faults. Second, weak grid conditions with $SCP_{bus1} < 3$ GVA amplify this displacement effect. The combined influence of high infeed and low short-circuit strength therefore explains the majority of missed in-zone faults. These findings confirm that static geometric zone settings cannot fully capture operating-point-dependent impedance shifts. Importantly, impedance deviations occur in both directions, implying that simply enlarging the protection zone would increase false positives without resolving the underlying sensitivity.

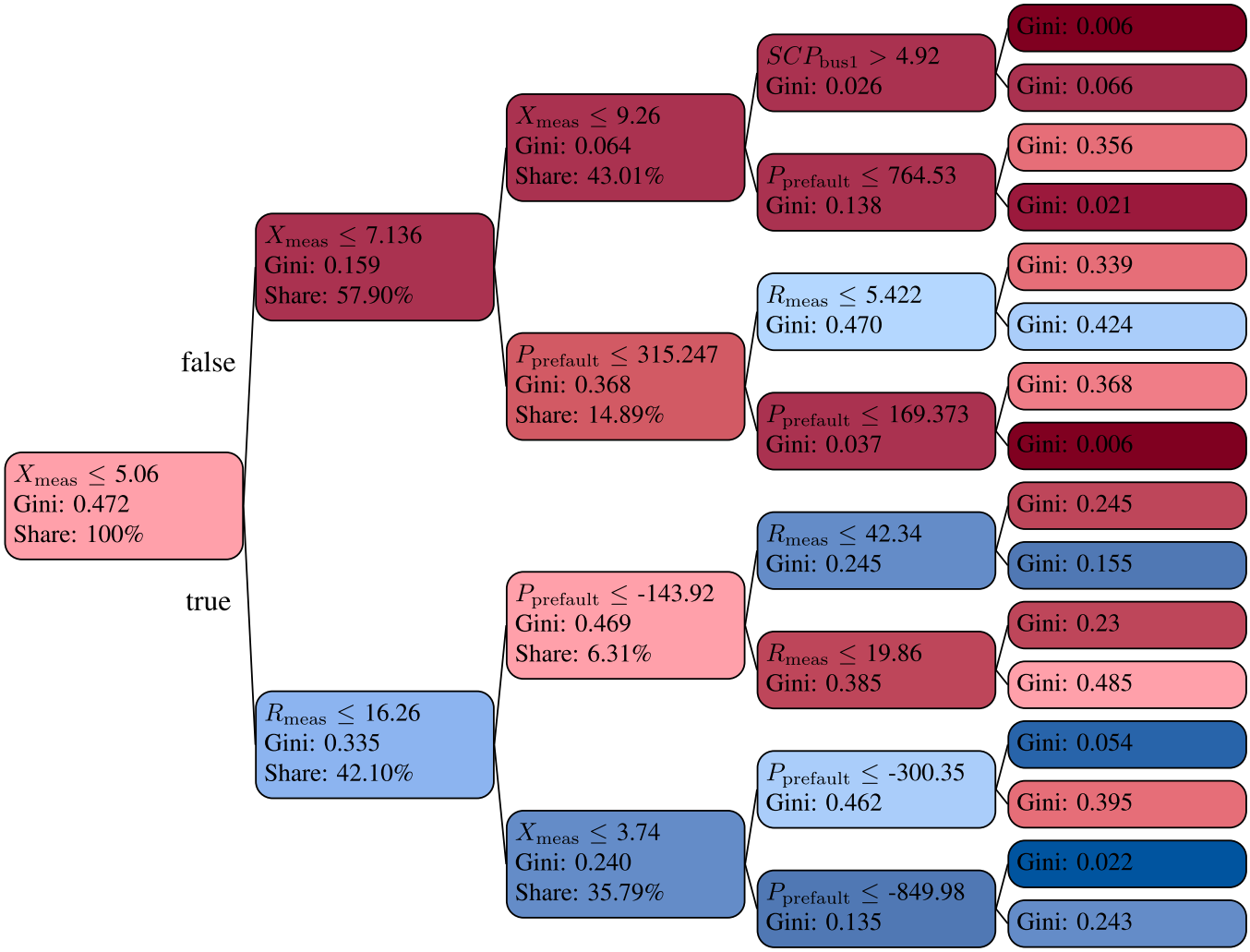


Fig. 6. Four-level decision tree derived from the distilled RF decision logic.

4.4. Performance evaluation and threshold optimisation of random forest classifiers

Accuracy does not peak at the conventional 80% reach setting but varies with the fault type. For 3ph-gnd faults, the accuracy-maximising threshold corresponds to an effective reach of 90.08%, yielding 93.6% accuracy, whereas for 1ph-gnd faults it corresponds to 77.58% reach with 90.1% accuracy. At these accuracy-maximising operating points, the corresponding dependability and security values for 3ph-gnd faults are 0.913 and 0.950, compared to 0.891 and 0.962 at the fixed 80% setting. For 1ph-gnd faults, dependability increases from 0.768 at 80% to 0.907 at the optimised threshold, while security decreases from 0.971 to 0.897. These shifts highlight the inherent trade-off between dependability and security, as defined in Eqs. (5) and (6), and confirm that fixed geometric reach settings cannot ensure balanced protection performance across fault types.

The ROC curves further quantify this trade-off by separating dependability (true positive rate) and security (1–false positive rate) over varying probability thresholds. Area-under-the-curve (AUC) values of 0.94 for 3ph-gnd faults and 0.91 for 1ph-gnd faults indicate strong separability between in-zone and out-of-zone cases across operating points. Figs. 9 and 12 summarise the classifier performance. The threshold–accuracy plot demonstrates that optimal reach depends on fault characteristics and operating conditions; static thresholds tied to fixed line percentages therefore cannot ensure optimal protection performance across all scenarios. Residual errors are predominantly false negatives under weak-grid conditions with high converter infeed, while false positives remain comparatively limited. Although the achieved accuracies indicate strong performance under simulated conditions, practical deployment requires further validation.

The study is limited to static simulations on the IEEE 14-bus system and does not explicitly account for measurement noise, dynamic converter control transients or communication delays. Overall, the results demonstrate that RF classification enables a shift from purely static geometric protection zones toward operating-condition-aware decision regions. By incorporating system indicators such as SCP and P_{prefault}, the framework enhances transparency and provides additional degrees of freedom to balance dependability and security. From a methodological standpoint, the proposed framework therefore differs from purely accuracy-driven machine-learning approaches in protection research. Rather than replacing conventional distance relays by a black-box classifier, the Random Forest is used to analyse how operating conditions reshape the effective Zone 1 decision boundary in protection-relevant terms. The combination of nonlinear modelling capability with intrinsic feature importance measures and SHAP-based explanations supports engineering interpretability while maintaining robustness against com-

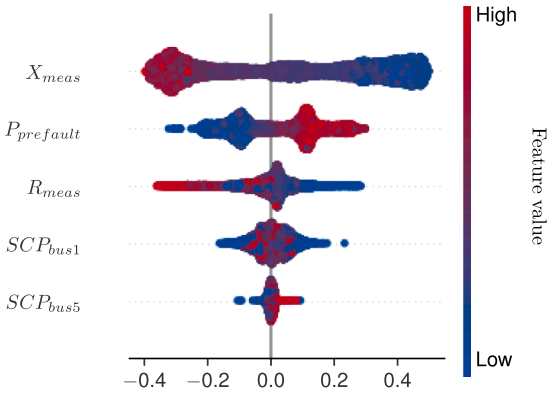


Fig. 7. SHAP beeswarm plot showing overall feature contributions for 3ph-gnd faults.

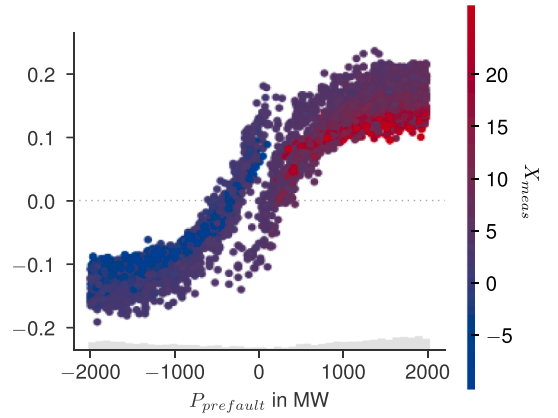


Fig. 8. Scatter distribution of misclassified 3ph-gnd faults with varying P_{prefault}.

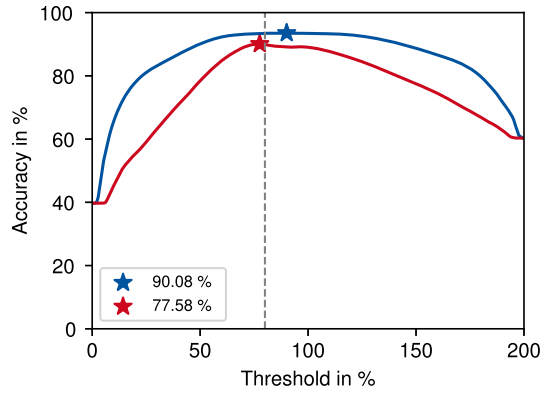


Fig. 9. Threshold-dependent accuracy of RF classifiers. Blue represents 3ph-gnd faults and red represents 1ph-gnd faults.

plex feature interactions. At the same time, the obtained results remain conditioned on the representativeness of the simulated scenarios and the static modelling assumptions outlined above.

5. Conclusion

Reliable distance protection may benefit from moving beyond static zone boundaries towards optimisation through Random Forest threshold tuning. Conventional relays with fixed settings cannot ensure dependable and secure operation in grids with high shares of converters, as apparent impedance trajectories are highly sensitive to short-circuit strength, pre-fault conditions and converter control. Analysis of large datasets with 100,000 simulated cases per fault type revealed system-

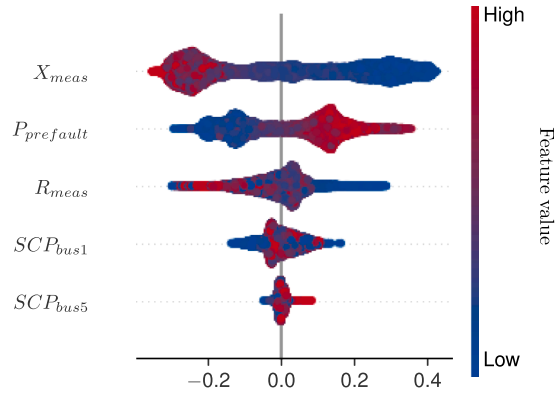


Fig. 10. SHAP beeswarm plot showing overall feature contributions for 1ph-gnd faults.

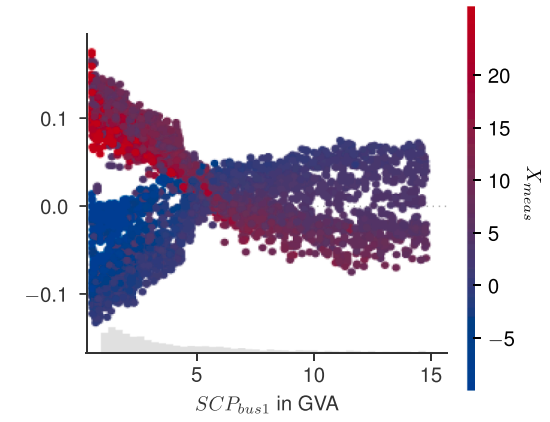


Fig. 11. Scatter distribution of misclassified 3ph-gnd faults with varying SCP_{bus1}.

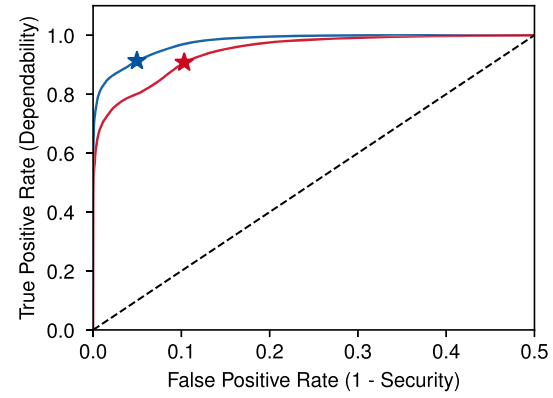


Fig. 12. ROC curves of RF classifiers for 3ph-gnd (blue) and 1ph-gnd (red) faults. Stars denote optimal thresholds achieving the best balance between dependability and security.

atic regions of misclassification and uncertainty near the Zone 1 boundary. SHAP-based feature attribution confirmed that apparent impedance components dominate the geometric decision, while short-circuit power and pre-fault converter load flow systematically shift the classification outcome under weak-grid conditions. Linking these insights to classical protection metrics provided a transparent connection between data-driven results and dependability and security. Incorporating system-aware features improved classification performance, with 3ph-gnd faults achieving accuracies up to 93.6% at an optimised threshold of 90.08% line coverage.

The proposed framework combines nonlinear modelling capability with interpretability through SHAP analysis and explicit threshold tuning to balance dependability and security. However, as a supervised data-driven method trained on offline simulations, its performance depends on the representativeness of the underlying scenarios. While a single decision tree offers higher transparency, its standalone accuracy remains below that of the full Random Forest ensemble, illustrating the trade-off between interpretability and predictive performance. Future work should address hyperparameter refinement, comparison with alternative classifiers, and extension to larger networks and transient dynamic simulations. In addition, validation using real disturbance records is required to assess robustness under practical operating conditions.

CRediT authorship contribution statement

Sarah Anhaus: Writing – review & editing, Writing – original draft, Visualization, Validation, Methodology, Investigation, Formal analysis, Data curation, Conceptualization; **Arlind Damjani:** Writing – review & editing, Conceptualization; **Willem Leterme:** Writing – review & editing, Supervision.

Declaration of competing interest

The authors declare that they have no known competing financial interests or personal relationships that could have appeared to influence the work reported in this paper.

Data availability

Data will be made available on request.

References

[1] R. Chowdhury, N. Fischer, Transmission line protection for systems with inverter-based resources — Part I: problems, IEEE Trans. Power Deliv. 36 (5) (2021) 2416–2425. https://doi.org/10.1109/TPWRD.2021.3062573

[2] V. Chakrapani, I. Voloh, P. Horton, S. Swain, Assessing the performance of an enhanced distance relay in converter-dominated network, in: 17th International Conference on Developments in Power System Protection (DPSP 2024), 2024, 2024, pp. 162–167. https://doi.org/10.1049/icp.2024.0892

[3] V. Hytti, P. Partinen, Performance of distance relays in the finnish power system under high penetration of converter-connected generation, CIGR/'E Paris Sess. 2024 (2024) B5-10105-2024.

[4] A. Hooshyar, M.A. Azzouz, E.F. El-Saadany, Distance protection of lines emanating from full-scale converter-interfaced renewable energy power plants—Part II: solution description and evaluation, IEEE Trans. Power Deliv. 30 (4) (2015) 1781–1791. https://doi.org/10.1109/TPWRD.2014.2369480

[5] S.I. Gkavanoudis, D. Tampakis, K. Malamaki, C.S. Demoulias, Protection philosophy in low short-circuit capacity distribution grids with high penetration of converter-interfaced distributed renewable energy sources, IET Gener. Transm. Distrib. 14 (22) (2020) 4978–4988. https://doi.org/10.1049/iet-gtd.2020.0714

[6] S. Paladhi, A.K. Pradhan, Adaptive fault type classification for transmission networks connecting converter-interfaced renewable plants, IEEE Syst. J. (2020). https://doi.org/10.1109/JSYST.2020.3010343

[7] K. Ma, Dissertation: Advanced Protection Schemes of Modern Power Systems with Converter Interface, Ph.D. thesis, Aalborg University, 2022.

[8] NREL, Overcurrent Limiting in Grid-Forming Inverters, Technical Report, NREL, 2024.

[9] S.M. Koloushani, S.A. Taher, Enhancing distance protection in transmission grids with high penetration of renewable energy sources through cooperative protection, IET Gener. Transm. Distrib. 18 (21) (2024) 3462–3475. https://doi.org/10.1049/gtd2.13295

[10] S.A. Khaparde, P.B. Kale, S.H. Agarwal, Application of artificial neural network in protective relaying of transmission lines, in: Proceedings of the First International Forum on Applications of Neural Networks to Power Systems, IEEE, 1991, pp. 122–125. https://doi.org/10.1109/ANN.1991.213509

[11] S.A. Khaparde, N. Warke, S.H. Agarwal, An adaptive approach in distance protection using an artificial neural network, Electr. Power Syst. Res. 37 (1) (1996) 39–44. https://doi.org/10.1016/0378-7796(96)01040-1

[12] A. Yadav, Y. Dash, An overview of transmission line protection by artificial neural network: fault detection, fault classification, fault location, and fault direction discrimination, Adv. Artif. Neural Syst. 2014 (2014) 1–20. https://doi.org/10.1155/2014/230382

[13] P. Gayashan, D. Kalana, C.J. Sebastian, V. Daniel, R. Athula, A review of machine learning applications in power system protection and emergency control: opportunities, challenges, and future directions, Front. Smart Grids. 3 - 2024 (2024) 2813–4311. https://doi.org/10.3389/frsgr.2024.1371153

[14] A.K. Ozcanli, F. Yaprakdal, M. Baysal, Deep learning methods and applications for electrical power systems: a comprehensive review, Int. J. Energy Res. 44 (9) (2020) 7136–7157. https://doi.org/10.1002/er.5331

[15] I. Alhamrouni, N.H. Abdul Kahar, M. Salem, M. Swadi, Y. Zahroui, D.J. Kadhim, F.A. Mohamed, M. Alhuyi Nazari, A comprehensive review on the role of artificial intelligence in power system stability, control, and protection: insights and future directions, Appl. Sci. 14 (14) (2024) 6214. https://doi.org/10.3390/app14146214

[16] J. Ma, H. Zhu, W. Xu, D. Fan, Application of ensemble learning in fault diagnosis and protection of smart grids, IEEE Trans. Smart Grid 12 (3) (2021) 2206–2215.

[17] A. Yazdaninejadi, H. Ebrahimi, S. Golshannavaz, An advanced local current-only protection for microgrids: deep-learning-based approach, IEEE Access 13 (2025) 56428–56438. https://doi.org/10.1109/ACCESS.2025.3555123

[18] A. Amraeimonfared, A. Yazdaninejadi, S. Teimourzadeh, Developing a new AI-based protection scheme for DER-integrated distribution networks: a techno-economic approach, IEEE Access 12 (2024) 164520–164531. https://doi.org/10.1109/ACCESS.2024.3491903

[19] H. Ebrahimi, S. Golshannavaz, A. Yazdaninejadi, E. Pouresmaeil, Improving protection reliability of series–compensated transmission lines by a fault detection method through an ML–based model, IET Gener. Transm. Distrib. 18 (21) (2024) 3452–3461. https://doi.org/10.1049/gtd2.13294

[20] M. Fayazi, A. Saffarian, M. Joorabian, M. Monadi, An AI-based fault detection and classification method for hybrid parallel HVAC/HVDC overhead transmission lines, Electr. Power Syst. Res. 238 (2025) 111083. https://doi.org/10.1016/j.epsr.2024.111083

[21] T. Hastie, R. Tibshirani, J. Friedman, The Elements of Statistical Learning, Springer, 2009.

[22] L. Breiman, Random forests, Mach. Learn. 45 (1) (2001) 5–32.

[23] G. Louppe, L. Wehenkel, A. Sutera, P. Geurts, Understanding variable importances in forests of randomized trees, Adv. Neural Inf. Process. Syst., vol. 26, 2013.

[24] S. Lundberg, S.-I. Lee, A unified approach to interpreting model predictions, in: Advances in Neural Information Processing Systems (NeurIPS), vol. 30, Curran Associates, Inc., Long Beach, CA, 2017.

[25] C. Molnar, Interpretable machine learning: a guide for making black box models explainable, Leanpub (2020). https://christophm.github.io/interpretable-ml-book/.

[26] W. Leterme, E. Heylen, Rethinking power system protection analysis and setting: introducing Bayesian analysis and decision theory, IEEE Trans. Power Deliv. 39 (1) (2024) 436–445. https://doi.org/10.1109/TPWRD.2023.3245148

[27] G. Ziegler, Numerical Distanceprotection: Principles and Application, Publicis-MCD-Verl., Erlangen, 1999.

[28] L. Thurner, A. Scheidler, F. Schäfer, J. Menke, J. Dollichon, F. Meier, S. Meinecke, M. Braun, Pandapower — an open-source python tool for convenient modeling, analysis, and optimization of electric power systems, IEEE Trans. Power Syst. 33 (6) (2018) 6510–6521. https://doi.org/10.1109/TPWRS.2018.2829021

[29] V.F. Rodriguez-Galiano, M. Sanchez-Castillo, M. Chica-Olmo, M. Chica-Rivas, Machine learning predictive models for mineral prospectivity: an evaluation of random forest and support vector machines, Ore Geol. Rev. 71 (2015) 804–818. https://doi.org/10.1016/j.oregeorev.2014.08.001

[30] L.S. Shapley, A value for n-person games, in: H.W. Kuhn, A.W. Tucker (Eds.), Contributions to the Theory of Games II, vol. 28 of Annals of Mathematics Studies, Princeton University Press, Princeton, NJ, 1953, pp. 307–317.

[31] R. Jinad, A. Islam, N. Shashidhar, Interpretability and transparency of machine learning in file fragment analysis with explainable artificial intelligence, Electronics 13 (13) (2024). https://doi.org/10.3390/electronics13132438

[32] T. Fawcett, An introduction to ROC analysis, Pattern Recognit. Lett. 27 (8) (2006) 861–874. https://doi.org/10.1016/j.patrec.2005.10.010